Journal of the Iranian Chemical Society (2025) 22:683–697
https://doi.org/10.1007/s13738-025-03177-0

ORIGINAL PAPER

# Syntheses, crystal structures, and DFT calculations of *N*'-(Pyridin-2-ylmethylene)nicotinohydrazide dihydrate and its copper complex

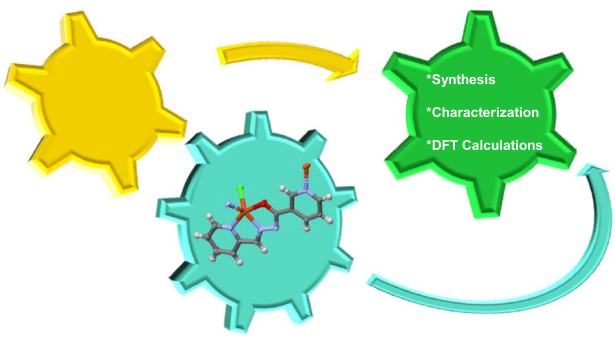
**Ömer Aydoğdu[1] · Füreya Elif Öztürkkan[2] · Tuncer Hökelek[3] · Güventürk Uğurlu[4] · Hacali Necefoğlu[1,5]**

Received: 31 January 2024 / Accepted: 12 January 2025 / Published online: 28 January 2025
© Iranian Chemical Society 2025

## Abstract

A Schiff base ligand, *N*'-(pyridine-2-ylmethylene)nicotinohydrazide dihydrate (**I**) and its Cu complex, *catena*-Poly[*N*'-(picolinylpyridine-3-carbohydrazonate)copper(II) (**II**) have been synthesized and their structures have been determined by $^{1}H$, $^{13}C$ NMR and FT-IR spectroscopies, elemental analysis and single crystal X-ray diffraction technique. The SCXRD analysis conforms the **I** crystallized in a Triclinic crystal system, with a $P-1$ space group and lattice parameters are $\alpha = 87.910$ (4)°, $\beta = 76.629$ (3)°, $\gamma = 80.769$ (3) °. **II** crystallized in an Orthorhombic crystal system, with a *Pbca* space group and lattice parameters, are $a = 8.6502$ (3) Å, $b = 11.4314$ (4) Å, and $c = 25.4146$ (6) Å, $\alpha$, $\beta$, $\gamma = 90°$. When the FT-IR spectra of the functional groups of the two synthesized compounds were examined, it was determined that the vibrations of the N–N and pyridine C–N groups observed in the spectra of Compound I were not observed in the same region in the spectra of Compound II and that chemical shifts occurred, and these chemical shifts were attributed to the Cu–N bonds. The Hirshfeld surface analyses have confirmed the importance of H-atom contacts in establishing the packings. The large number of H–H, H–N/N–H, H–C/C–H, H–O/O–H, H–Cl/Cl–H and C–C interactions have been suggested that van der Waals interactions and hydrogen bonding play major roles in the crystal packings. In addition, geometric optimizations of both synthesized compounds were made and the electronic, nonlinear optical (NLO) property and vibration frequencies of the compounds in equilibrium were examined theoretically. The calculations of compound **I** were performed with both DFT/B3LYP and HF methods using the 6–311 + + G(d,p) basis set but calculations on compound **II** are predicted at DFT/B3LYP level by using a mixed basis set of LANL2DZ (for Cu) and 6-311G (for other atoms). The dipole moment of compound **I** is calculated as 4.30 Debye at the DFT/B3LYP/6–311 + + G(d,p)and 3.57 Debye HF/6–311 + + G(d,p) level of theory, respectively.

## Graphical abstract




**Keywords** Schiff base · N-donor ligand · Nicotinic hydrazide · Cu(II) complex · DFT

Extended author information available on the last page of the article

## Introduction

Schiff bases are imine-containing compounds formed by the condensation of primary amine and active carbonyl compounds. The azomethine group is a structural characteristic maintained in many compounds, with the general formula RHC = N-R', where R and R' are alkyl, aryl, cycloalkyl, or heterocyclic groups that can be replaced in numerous ways. Schiff bases are also referred to as anils, imines, or azomethines [1, 2]. Schiff bases can be defined as both an important class of organic compounds and a powerful class of ligands of coordination chemistry due to their strong coordination abilities. It can form complexes with metals because Schiff base ligands exhibit the ability to form stable complexes with metal ions through the N-, O-, and S-donor atoms in their structures [3–6]. Transition metal complexes form interesting complexes with almost all ligand classes [7, 8]. These properties are also valid for complexes with Schiff base ligands [9–11]. Schiff bases are effective chelating agents for metal ions, allowing them to coordinate and form stable complexes. Copper is a notable metal because of the wide range of structural chemistry it exhibits, with coordination numbers that range from 4 to 6. Due to differences in their structural chemistry, copper complexes formed from Schiff bases have been studied throughout the last decade [12–14]. Copper complexes of hydrazones, which are excellent multidentate chelating ligands, have been determined to have both stable structures and unique biologically active potentials [15–17]. The exploration of Schiff base complexes, particularly those involving tridentate ONO ligands, has garnered significant attention in the field of coordination chemistry due to their diverse applications in catalysis and material science. Recent studies have focused on the synthesis, characterization, and catalytic properties of various metal complexes incorporating these ligands, revealing their potential to facilitate organic transformations. The synthesis and characterization of Schiff base complexes, particularly those with tridentate ONO ligands, reveal their significant role in catalysis. The previous studies demonstrate that the structural and electronic properties of the ligands are pivotal in determining the catalytic activity of the metal complexes, thereby paving the way for future research in this domain [18–25]. Because of their unique characteristics and wide range of uses, Schiff bases, and their copper complexes have attracted a lot of interest in the fields of coordination chemistry and materials science. Schiff bases, which are created when primary amines are condensed with carbonyl compounds, have a variety of coordination properties, especially when it comes to transition metals like copper. The structural variety and biological activity of the resultant copper(II) complexes make them notable. The nature of the Schiff base ligands affects the structural properties of copper(II) Schiff base complexes. Ma et al., for example, emphasize the significance of these complexes as stereochemical models in transition metal coordination chemistry, demonstrating their structural diversity and simplicity of production. The nitrogen and oxygen donor atoms are usually involved in the coordination of copper ions with Schiff bases, resulting in a variety of geometries, such as square planar and tetrahedral configurations [26–28]. In conclusion, the structural diversity, outstanding biological activities, and possible uses in materials science and catalysis define the characteristics of Schiff bases and their copper complexes. The continuous investigation of these complexes keeps shedding light on their modes of action and expanding their range of applications. Based on this, we report the synthesis, characterization, and crystal structure of a novel Schiff base ligand of *N'*-(pyridine-2-ylmethylene)nicotinohydrazide (**I**) and its complex *catena*-Poly[N'-(picolinylpyridine-3-carbohydrazonate)copper(II) (**II**). The molecular structures of the synthesized compounds were determined using the single-crystal X-ray diffraction technique, elemental analysis, $^{1}H$ and $^{13}C$ NMR, and UV–Vis spectroscopies. It is known that the common characterization methods for Schiff bases are FT-IR and NMR spectroscopy. There are more limited data on their crystal structures. For this purpose, in this study, crystal data of both the synthesized organic ligand and its copper complex are presented. In addition, theoretical properties of both synthesized compounds are investigated in detail by DFT studies. With the use of DFT, the optimized structure, HOMO–LUMO energy gap, MEP, and NLO properties of these compounds were all clearly described.

## Materials and methods

### Chemicals and instruments

Copper(II) chloride dihydrate ($CuCl_2{\cdot}2H_2O$), methanol, glacial acetic acid, 2-pyridinecarboxyaldehyde and nicotinic hydrazide (Sigma-Aldrich, Türkiye) were purchased commercially and used without prior purification. Infrared spectra of the compounds were recorded from solid samples on an Alpha-P BRUKER Infrared (FT-IR) Spectrometer at 400–4000 $cm^{-1}$. Compounds were dissolved in DMSO and $^{1}H$ and $^{13}C$ NMR spectra were recorded with device Agilent 400 MHz. Elemental percentages of C, H, and N were determined using a Thermo Scientific, Flash 2000 elemental analyzer. UV–Vis spectra of the compounds were taken with a Perkin Elmer Lambda 25 UV–Vis Spectrophotometer using samples dissolved in DMF.

### Synthesis of N'-(Pyridin-2-ylmethylene)nicotinohydrazide dihidyrate (I)

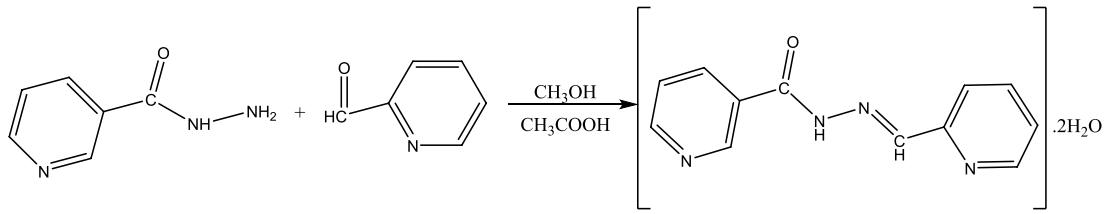
Nicotinic hydrazide (1.25 g, 0.009 mol), placed in a round-bottomed 250 mL flask was dissolved in methanol (50 mL). Then, 2-pyridinecarboxyaldehyde (0.976 g, 0.009 mol) was dissolved in methanol (20 mL) and added into the flask with nicotinic hydrazide solution dissolved in methanol. 5–6 drops of glacial acetic acid were added to this mixture. The resulting mixture was mixed under a reflux device at 80 °C for 6–8 h. After the reaction was completed, the solution was kept at room temperature. Yellow crystals precipitated from the solution and were filtered. Anal. Calc. (%) for $C_{12}H_{10}N_4O{\cdot}2H_2O$: C, 54.95; H, 5.38; N, 21.36. Found (%): C, 54.47; H, 5.95; N, 21.03. Yield: 87%. FT-IR ($cm^{-1}$); $\nu$(N–H): 3100, $\nu$(C-H)ring: 2844, $\nu$(C=O): 1666, $\nu$(C=N): 1591, $\nu$(C–N):1290. $^1$H-NMR (400 MHz, ppm, $d_6$-DMSO) δ $^1$H-NMR δ 12.23 (s, 1H), 9.08 (d, $J = 1.5$ Hz, 1H), 8.78–8.73 (m, 1H), 8.59 (d, $J = 4.6$ Hz, 1H), 8.45 (s, 1H), 8.29–8.23 (m, 1H), 7.98 (d, $J = 7.9$ Hz, 1H), 7.86 (td, $J = 7.8$, 1.3 Hz, 1H), 7.55 (dd, $J = 7.9$, 4.9 Hz, 1H), 7.42–7.36 (m, 1H). $^{13}$C-NMR (100 MHz, ppm, $d_6$-DMSO) δ 162.5, 153.4, 152.9, 150.0, 149.1, 149.1, 137.3, 136.0, 129.4, 125.0, 124.1, 120.5 (Schemes 1 and 2).

### Synthesis of catena-poly[N'-(picolinylpyridine-3-carbohydrazonate)copper(II) (II)

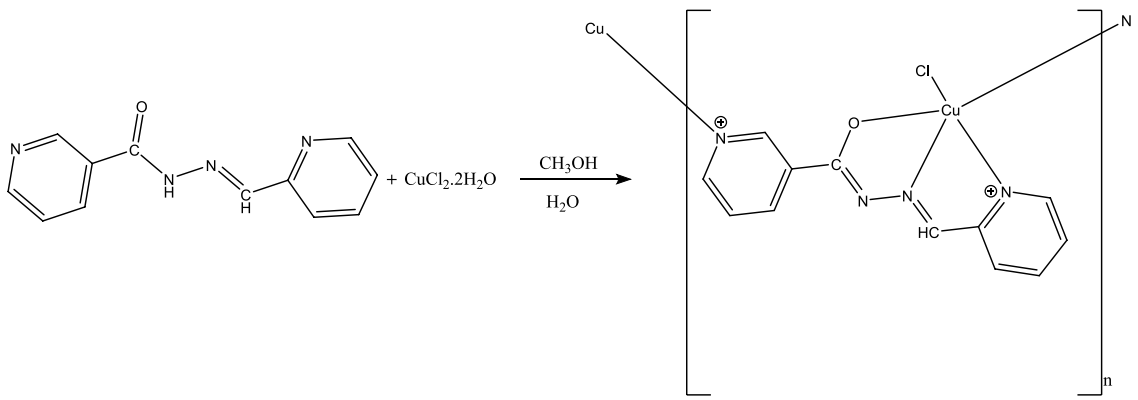
In a beaker, 1.13 g (0.005 mol) of *N′*-(Pyridin-2-ylmethylene)nicotinohydrazide dihydrate (**I**) compound was dissolved in 20 mL of methanol. In a separate beaker, 0.42 g (0.0025 mol) copper (II) chloride dihydrate, $CuCl_2.2H_2O$, was dissolved in a mixture of 50 mL distilled water and methanol (1:1). *N*'-(Pyridin-2-ylmethylene)nicotinohydrazide dihydrate Schiff base compound solution was added into the $CuCl_2.2H_2O$ solution and kept at room temperature. The green crystals formed after 5 days were filtered. Anal. Calc. (%) for $C_{12}H_9ClCuN_4O$: C, 44.45; H, 2.79; N, 17.28. Found (%): C, 44.91; H, 2.47; N, 17.89. FT-IR ($cm^{-1}$); $\nu$(C–H)ring: 2844, $\nu$(C=N): 1369, $\nu$(C–N):1158.

### X-ray crystallography

The crystallographic data of the compounds (**I** and **II**) were collected on a Bruker APEX-II CCD diffractometer using Mo$K_\alpha$ radiation ($\lambda = 0.71073$ Å). The data were processed by SHELX program packages [*SHELXT 2018/2* [29] and *SHELXL 2018/2* [30]] for solving and refining the structures, and ORTEP-3 [31] and PLATON [32] programs were used in drawings. The water hydrogens (for **I**) were located in difference Fourier maps and refined by applying some restrains and constrains. The remaining hydrogen atom positions were




**Scheme 1** Synthesis of *N*'-(Pyridin-2-ylmethylene)nicotinohydrazide dihydrate (**I**)




**Scheme 2** Synthesis of *catena*-poly[*N*'-(picolinylpyridine-3-carbohydrazonate)copper(II) (**II**)

**Table 1** Experimental details for compounds (**I** and **II**)

| Compound | (I) | (II) |
|---|---|---|
| *Crystal data* | | |
| Chemical formula | $C_{12}H_{10}N_4O{\cdot}2(H_2O)$ | $C_{12}H_9ClCuN_4O$ |
| $M_r$ | 262.27 | 324.22 |
| Crystal system, space group | Triclinic, *P* -1 | Orthorhombic, *Pbca* |
| Temperature (K) | 296 | 296 |
| *a*, *b*, *c* (Å) | 6.4306 (3), 7.9904 (3), 12.9507 (5) | 8.6502 (3), 11.4314 (4), 25.4146 (6) |
| α, β, γ (°) | 87.910 (4), 76.629 (3), 80.769 (3) | 90 |
| *V* (Å$^3$) | 639.02 (5) | 2513.09 (14) |
| *Z* | 2 | 8 |
| Radiation type | Mo *K*α | Mo *K*α |
| μ (mm$^{-1}$) | 0.10 | 1.95 |
| Crystal size (mm) | 0.11 × 0.07 × 0.06 | 0.10 × 0.09 × 0.05 |
| *Data collection* | | |
| Diffractometer | Bruker *APEX*-II CCD | Bruker *APEX*-II CCD |
| Absorption correction | – | – |
| No. of measured, independent and observed [$I > 2\sigma(I)$] reflections | 19,820, 3189, 2240 | 19,907, 3114, 2060 |
| $R_{int}$ | 0.041 | 0.079 |
| $(\sin\theta/\lambda)_{max}$ (Å$^{-1}$) | 0.669 | 0.667 |
| *Refinement* | | |
| $R[F^2 > 2\sigma(F^2)]$, $wR(F^2)$, *S* | 0.049, 0.143, 1.02 | 0.075, 0.147, 1.09 |
| No. of reflections | 3189 | 3114 |
| No. of parameters | 188 | 172 |
| H-atom treatment | H atoms treated by a mixture of independent and constrained refinement | H atoms treated by a mixture of independent and constrained refinement<br>$w = 1/[\sigma^2(F_o^2) + (0.0185P)^2 + 17.09\,17P]$ where $P = (F_o^2 + 2F_c^2)/3$ |
| $\Delta\rho_{max}$, $\Delta\rho_{min}$ (e Å$^{-3}$) | 0.28, − 0.18 | 0.57, − 0.76 |

calculated geometrically at distances of 0.86 Å (for NH in **I**) and 0.93 Å (for aromatic CH) and refined using a riding model by applying the constraints of $U_{iso}(H) = 1.2 \times U_{eq}$ (C, N). Crystallographic data for the structure reported herein have been deposited with the Cambridge Crystallographic Data Centre as Supporting Information, **CCDC Nos.** 2239064 (for **I**) and 2,239,065 (for **II**). Copies of the data can be obtained through application to CCDC, 12 Union Road, Cambridge CB2 1EZ, UK. (fax: + 44 1223 336,033 or e-mail: deposit@ccdc.cam.ac.uk or at http://www.ccdc.cam.ac.uk).

## Computational details

All theoretical calculations regarding the compounds were made in the gas phase with the help of the Gaussian 09W program package and Gauss View 5.0 molecular visualization programs [33, 34]. The calculations of compound **I** were performed both DFT [35, 36] with B3LYP, which is a 3-parameter Becke mixed model with Lee–Yang–Parr (LYP) [37–39] and HF [40] using 6–311 + + G(d,p) basis set [41, 42] but calculations on compound **II** are predicted at DFT/B3LYP level by using LANL2DZ and a mixed basis set of LANL2DZ [43–45] (for Cu) and 6-311G (for other atoms). The molecular electrostatic potential surface (MEP), the frontier orbitals (HOMO—Highest Occupied Molecular Orbital), (LUMO—Lowest Unoccupied Molecular Orbital) of compound **I** have been calculated both DFT-B3LYP/6–311 + + G(d,p) and HF/6–311 + + G(d,p) level of theory. The calculated vibration frequencies were scaled with appropriate scale factors [46] and the assigning of these wavenumbers was done using the VEDA 4f program [47].

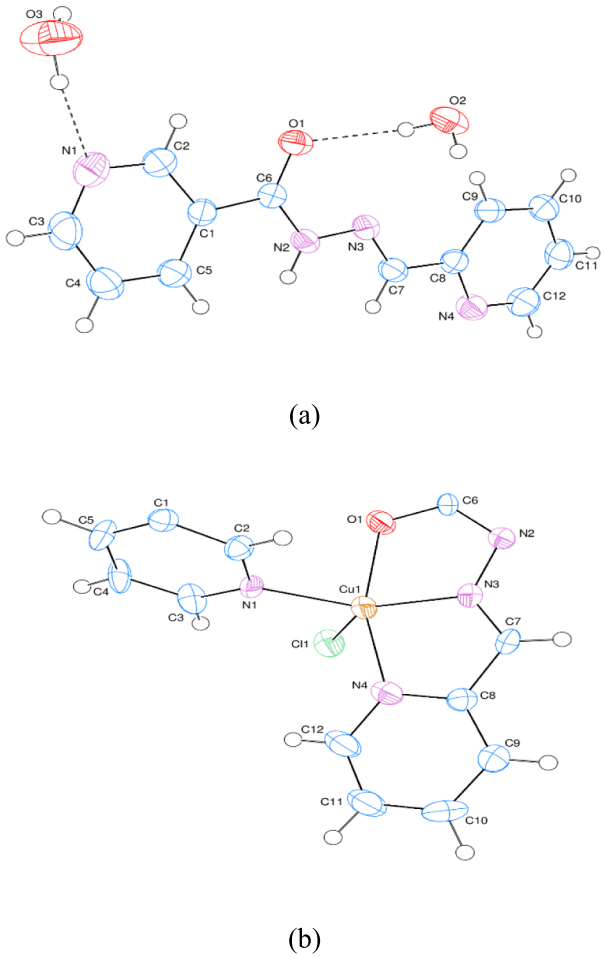



**Fig. 1** The asymmetric units of compounds **a I** and **b II** with the atom numbering schemes. Thermal ellipsoids are drawn at the 50% probability level. The O–H–O and O–H–N hydrogen bonds are shown as dashed lines (for **I**)

## Results and discussion

### X-Ray structures

The experimental details for compounds (**I** and **II**) are given in Table 1. In the asymmetric unit of compound **I** (Fig. 1a), there are two uncoordinated water molecules, linking to the ligand through the O–H–N and O–H–O hydrogen bonds, where the planar *A* (N1/C1–C5) and *B* (N4/C8–C12) rings are oriented at a dihedral angle of 11.61 (5)°. In the asymmetric unit of compound **II** (Fig. 1b), the $Cu^{II}$ atom is coordinated by two pyridine nitrogen, one hydrazone nitrogen, and one oxygen of the planar pyridine nicotinoylhydrazone group and one chloride anion. The Cu1–O1 and Cu1–Cl1 bond lengths are 1.975 (4) Å and 2.3676 (17) Å, while the Cu1–N1, Cu1–N3 and Cu1–N4 bonds are 2.101 (4) Å, 1.945 (4) Å and 2.036 (5) Å, respectively. $Cu^{II}$ atom adopts a highly distorted square pyramidal geometry, where three nitrogen atoms (N1, N3, and N4) and one oxygen atom (O1) occupy the base positions, and the apical position is occupied by the chlorine atom (Cl1) (Figs. 1b and 2). The one-dimensional polymeric structure is formed through the nicotinyl ligand bridging the $Cu^{II}$ centers along the *a*-axis direction (Fig. 2). The pyridine nicotinoylhydrazone group is almost planar with a maximum deviation of 0.075 (5) Å for atom N4 from the best least-squares plane, and it is oriented with respect to the pyridine ring A (N1/C1–C5) at a dihedral angle of 68.43(11)°.

In the crystal structure of **I**, the C–H–O, N–H–O, O–H–N and O–H–O hydrogen bonds (Table 2) link the molecules into a three-dimensional architecture (Fig. 3a), in which they may be effective in the stabilization of the structure. π–π interactions [centroid to centroid distance = 3.8382(9) Å] between the parallel pyridine rings further stabilize the structure. There is not any C–H-π interaction. In the crystal

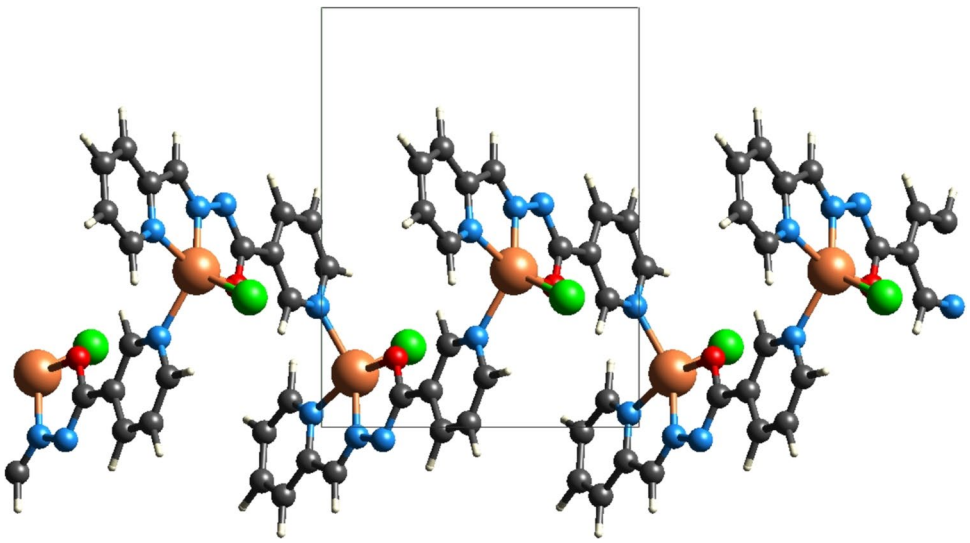


**Fig. 2** The one-dimensional polymeric structure of compound **II** is viewed down the *c*-axis direction, where the *a*-axis is horizontal and *b*-axis is vertical

**Table 2** Hydrogen-bond geometry (Å, °) for compound I

| *D*–H–*A* | *D*–H | H–*A* | *D*–*A* | *D*–H–*A* |
|---|---|---|---|---|
| N2–H2A–O2$^{i}$ | 0.86 | 2.03 | 2.8609 (18) | 162 |
| O2–H21–N4$^{ii}$ | 0.85 (3) | 2.07 (3) | 2.900 (2) | 165 (3) |
| O2–H22–O1 | 0.88 (3) | 2.06 (3) | 2.8889 (18) | 157 (2) |
| O3–H31–N1 | 0.96 (4) | 2.00 (4) | 2.945 (2) | 171 (3) |
| O3–H32–O1$^{iii}$ | 0.80 (4) | 2.43 (4) | 3.136 (2) | 147 (3) |
| O3–H32–N3$^{iii}$ | 0.80 (4) | 2.49 (4) | 3.192 (2) | 147 (4) |
| C5–H5–O2$^{i}$ | 0.93 | 2.48 | 3.373 (2) | 161 |
| C7–H7–O2$^{i}$ | 0.93 | 2.45 | 3.245 (2) | 144 |
| C12–H12–O3$^{iv}$ | 0.93 | 2.52 | 3.350 (3) | 149 |

(i) $x+1, y, z$; (ii) $-x+1, -y+1, -z+2$; (iii) $-x+1, -y+1, -z+1$; (iv) $x, y+1, z+1$

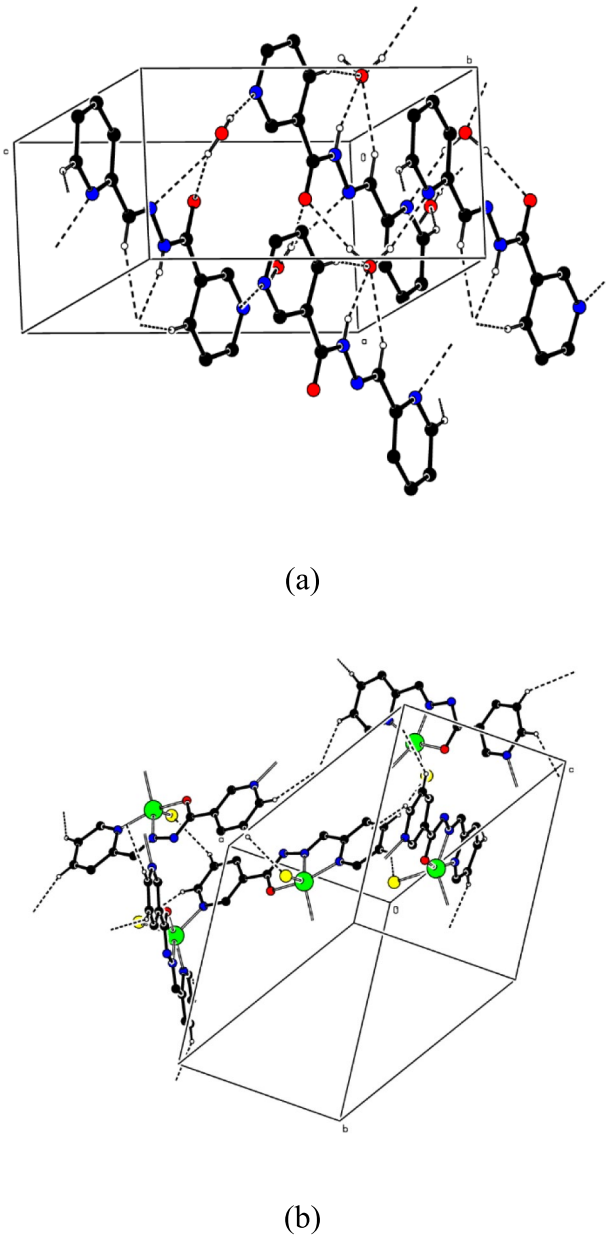
structure of **II**, the C–H–Cl hydrogen bonds (Table 3) link the molecules, enclosing $R_2^2(16)$ ring motifs [48], into a three-dimensional architecture (Fig. 3c), in which they may be effective in the stabilization of the structure. Neither π–π nor C–H–π interactions are observed.

It has been determined that the data on bond lengths and angles determined by single crystal X-ray diffraction of compound **I** are compatible with the data on bond lengths and angles calculated by both DFT and HF (Table S1).

Using the DFT/B3LYP level by using the LANL2DZ basis set, bond lengths for Cu1–O1 and Cu1–Cl1 were calculated as 2.283 Å and 2.017 Å, respectively. Using the same basis set, the Cu1–N3 and Cu1–N4 bond lengths were found to be 2000 Å and 2057 Å. Data regarding all other bond lengths and angles found by single crystal X-ray diffraction of the complex are also similar to the calculated data (Table S2). These results, which are consistent with each other, show that the LANL2DZ basis set is an ideal basis set for metal complexes.

## Hirshfeld surface analysis

To visualize the intermolecular interactions in the crystals of the compounds (**I** and **II**), Hirshfeld surface (HS) analyses [49, 50] were carried out by using Crystal Explorer 17.5 [51]. In the HS plotted over $d_{norm}$ (Fig. 4a–c), the white surface indicates contacts with distances equal to the sum of van der Waals radii, and the red and blue colors indicate distances shorter (in close contact) or longer (distinct contact) than the van der Waals radii, respectively [52]. The shape index of the HS is a tool to visualize the π–π stacking by the presence of adjacent red and blue triangles; if there are no adjacent red and/or blue triangles, then there are no π–π interactions. Figure 5a–c suggests that there are π–π interactions only in compound **I**. The overall two-dimensional fingerprint plots, Fig. 6a–b *a*, and those delineated into H–H, H–O/O–H, H–C/C–H, H–N/N–H, C–C, C–N/N–C,



(a)

(b)

**Fig. 3** The partial packing diagrams of compounds **a I** and **b II**. The C–H–O, N–H–O, O–H–N and O–H–O (for **I**) and the C–H–Cl (for **II**) hydrogen bonds are shown as dashed lines. The nonbonding hydrogen atoms have been omitted for clarity

**Table 3** Hydrogen-bond geometry (Å, °) for compound II

| *D*–H–*A* | *D*–H | H–*A* | *D*–*A* | *D*–H–*A* |
|---|---|---|---|---|
| C3–H3–Cl1 | 0.93 | 2.69 | 3.321 (6) | 126 |
| C4–H4–Cl1$^{iv}$ | 0.93 | 2.77 | 3.547 (6) | 142 |
| C10–H10–Cl1$^{iii}$ | 0.93 | 2.82 | 3.664 (8) | 151 |
| C11–H11–Cl1$^{ii}$ | 0.93 | 2.69 | 3.471 (7) | 142 |

(ii) $x-1/2, y, -z+3/2$; (iii) $-x+1, y+1/2, -z+3/2$; (iv) $-x+3/2, y-1/2, z$

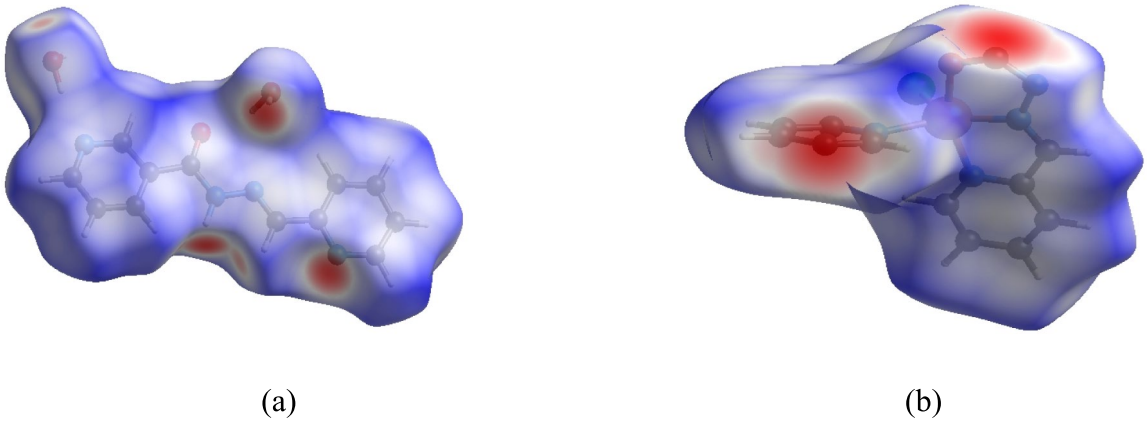



**Fig. 4** Views of the three-dimensional Hirshfeld surfaces of compounds **a I** and **b II** plotted over $d_{norm}$ in the ranges of -0.5559 to 1.1755 a.u. (for **I**) and − 1.1281 to 1.1467 a.u. (for **II**)

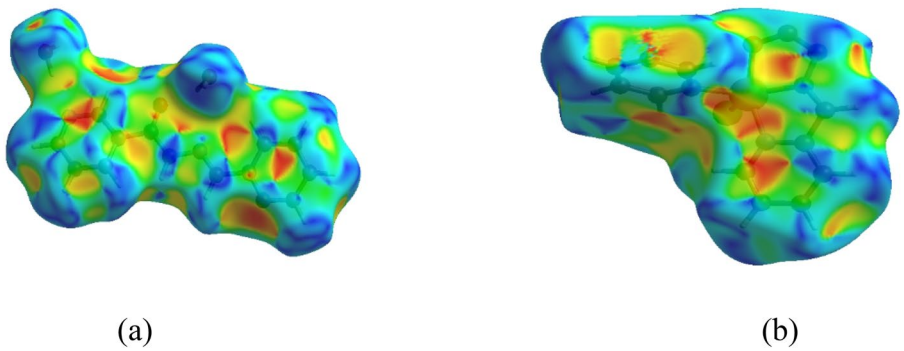



**Fig. 5** Hirshfeld surfaces of compounds **a I** and **b II** plotted over shape-index

N–N and C–O/O–C (for compound **I**) and H–H, H–Cl/Cl–H, H–C/C–H, C–C, H–N/N–H, H–O/O–H, C–N/N–C, N–N, C–Cl/Cl–C, N–O/O–N, C–O/O–C and H–Cu/Cu–H (for compound **II**) contacts [53] are illustrated in Fig. 6a *b–i* (for compound **I**) and Fig. 6b *b–m* (for compound **II**) together with their relative contributions to the Hirshfeld surfaces. The most important interactions, H–H contributing 44.4% (for **I**) and 33.3% (for **II**) to the overall crystal packings are reflected in Fig. 6a–b *b* as the widely scattered points of high density due to the large hydrogen contents of the molecules with the tips at $d_e = d_i = 1.16$ Å (for **I**) and $d_e = d_i = 1.17$ Å (for **II**). The pairs of spikes in the fingerprint plots delineated into H–O/O–H contacts have symmetrical distributions of points contributing 20.9% (for **I**) and 7.3% (for **II**) to the HSs, and they are reflected in Fig. 6a *c* (for **I**) and Fig. 6b *g* (for **II**) with the tips at $d_e + d_i = 1.87$ Å (for **I**) and $d_e + d_i = 2.40$ Å (for **II**). In the presence (for **I**) and absence (for **II**) of C–H–π interactions, the H–C/C–H contacts contributing 10.4% (for **I**) and 13.3% (for **II**) to the overall crystal packings, are reflected in Fig. 6a and b d (for **I** and **II**) with the tips of the wings at $d_e + d_i = 3.00$ Å (for **I**) and $d_e + d_i = 3.32$ Å (for **II**). The H–N/N–H contacts appearing in Fig. 6a *e* (for **I**) and Fig. 6b f (for **II**) have contributions of 10.0%, 16.2% and 9.7%, respectively, to the HSs with the tips at $d_e + d_i = 1.92$ Å (for **I**) and $d_e + d_i = 2.52$ Å, $d_e + d_i = 1.12$ Å (for tiny one) and $d_e + d_i = 3.31$ Å, from left to right (for **II**). The C–C contacts have bullet-shaped (for **I**) and needle-shaped (for **II**) distributions of points, and they are shown in Fig. 6a f (for **I**) and Fig. 6b e (for **II**) with the tips at $d_e = d_i = 1.73$ Å (for **I**) and $d_e = d_i = 0.73$ Å (for **II**). The C–N/N–C contacts have contributions of 5.4% (for **I**) and 3.7% (for **II**) to the HSs, and they are shown in Fig. 6a g (for **I**) and Fig. 6 b *h* (for **II**) with the tips at $d_e + d_i = 3.45$ Å (for **I**) and $d_e = d_i = 2.40$ Å (for **II**). The N–N contacts [Fig. 6a g (for **I**) and Fig. 6b i(for **II**)] contributions to the HSs are 0.9% (for **I**) and 2.0% (for **II**) with the tips at $d_e + d_i = 3.49$ Å (for **II**). The H–Cl/Cl–H [14.7%, Fig. 6b c] and C–Cl/Cl–C [2.0%, Fig. 6b j] (for **II**) contacts have distributions of points with the tips at $d_e + d_i = 2.54$ Å and $d_e + d_i = 3.41$ Å, respectively. The C–O/O–C [Fig. 6a h (for **I**)] and Fig. 6b l (for **II**)], N–O/O–N [Fig. 6b k (for **II**)] and H–Cu/Cu–H [Fig. 6b m (for **II**)] contributions to the HSs are smaller than 1.0% with scattered points of very low densities.

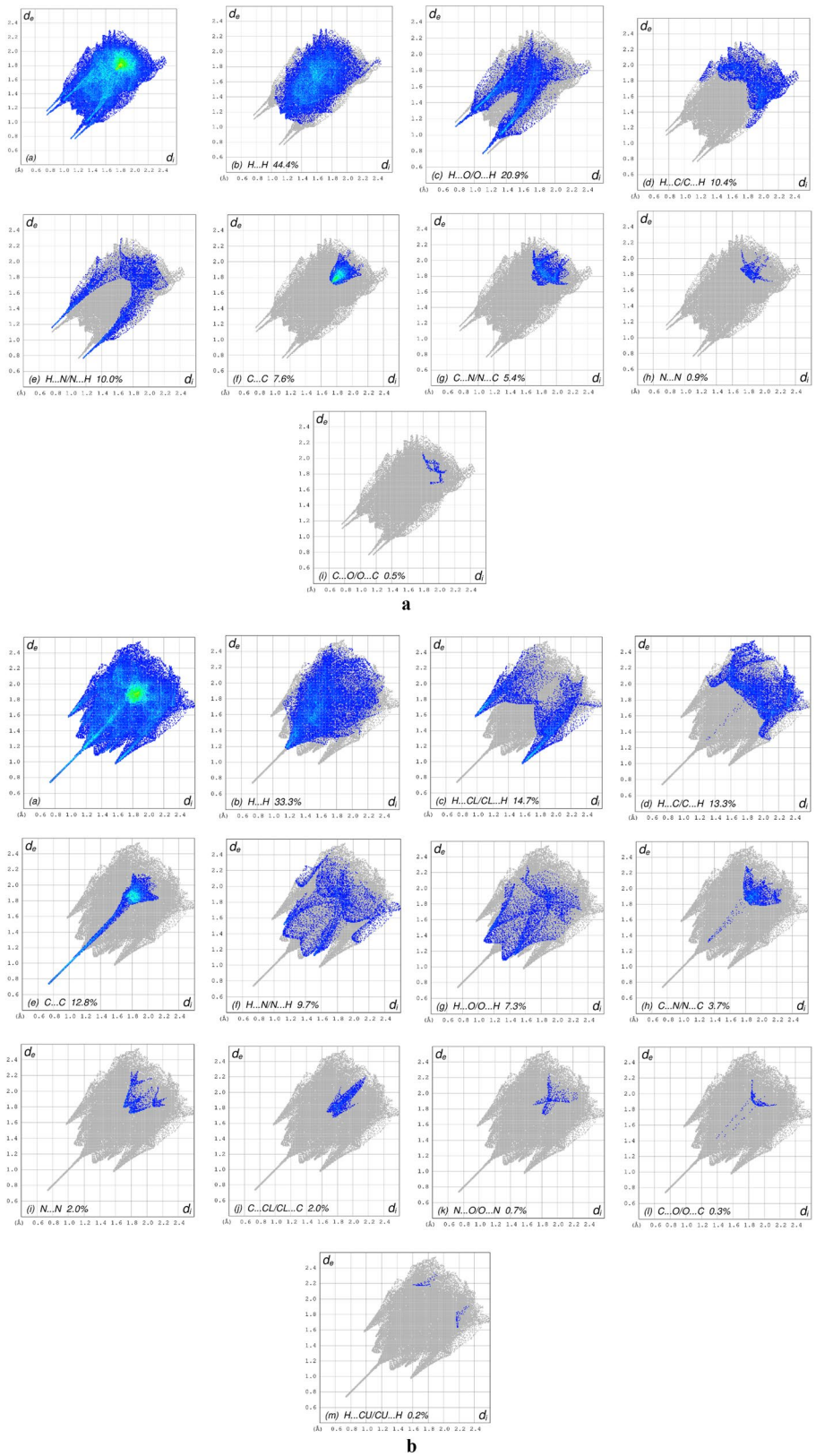



**Fig. 6** **a** The full two-dimensional fingerprint plots for compound **I**, showing all interactions (**a**), and delineated into H–H (**b**), H–O/O–H (**c**), H–C/C–H (**d**), H–N/N–H (**e**), C–C (**f**), C–N/N–C (**g**), N–N (**h**) and C–O/O–C (**i**) interactions. The $d_i$ and $d_e$ values are the closest internal and external distances (in Å) from given points on the Hirshfeld surface contacts. **b** The full two-dimensional fingerprint plots for compound **II**, showing all interactions (**a**), delineated into H–H (**b**), H–Cl/Cl–H (**c**), H–C/C–H (**d**), C–C (**e**), H–N/N–H (**f**), H–O/O–H (**g**), C–N/N–C (**h**), N–N (**i**), C–Cl/Cl–C (**j**), N–O/O–N (**k**), C–O/O–C (–l) and H–Cu/Cu–H (**m**) interactions. The $d_i$ and $d_e$ values are the closest internal and external distances (in Å) from given points on the Hirshfeld surface contacts

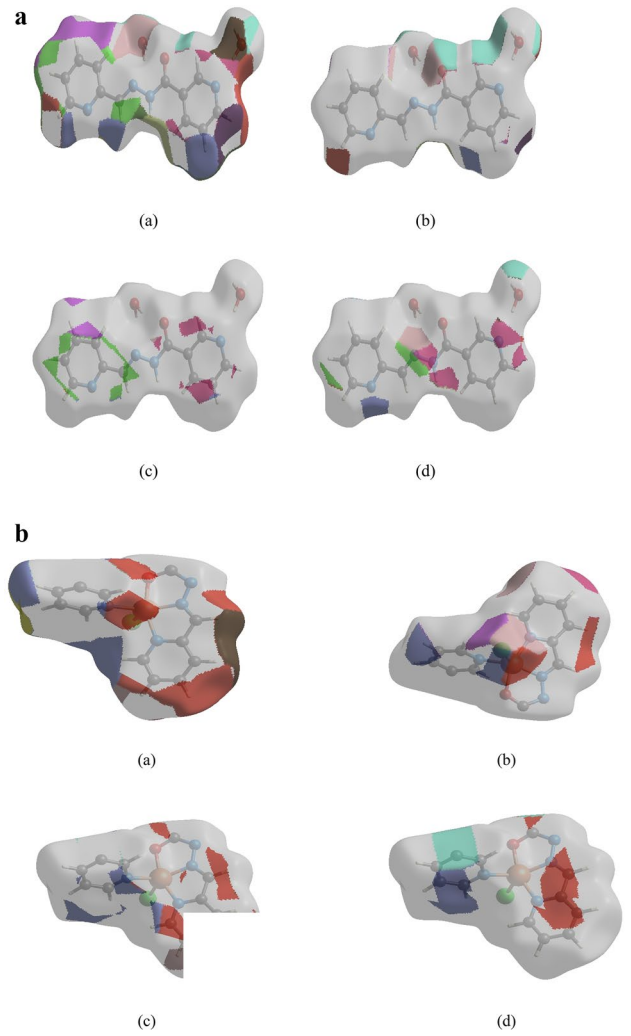



**Fig. 7** **a** The Hirshfeld surface representations of compound **I** with the function $d_{norm}$ plotted onto the surface for **a** H–H, **b** H–O/O–H, (c) H–C/C–H and (d) H–N/N–H interactions. **c** The Hirshfeld surface representations of compound **II** with the function $d_{norm}$ plotted onto the surface for (a) H–H, (b) H–Cl/Cl–H, (c) H–C/C–H and (d) C–C interactions

The nearest neighbor coordination environment of a molecule can be determined from the color patches on the HS based on how close to other molecules they are. The Hirshfeld surface representations with the function $d_{norm}$ plotted onto the surface are shown for the H–H, H–O/O–H, H–C/C–H and H–N/N–H (for **I**) and H–H, H–Cl/Cl–H, H–C/C–H and C–C (for **II**) interactions in Fig. 7a–b.

The Hirshfeld surface analyses confirm the importance of H-atom contacts in establishing the packings. The large number of H–H, H–O/O–H, H–C/C–H, H–N/N–H and H–Cl/Cl–H interactions suggest that van der Waals interactions and hydrogen bonding play major roles in the crystal packings [54]. Many studies have reported that hydrogen bonds and π–π stacking interaction between the molecules contribute significantly to the stability of the crystal packing [55–60].

## Crystal voids

The strength of the crystal packing is highly important to respond to the applied mechanical force depending on "how crystal packing is strong." Of course, if the crystal packing has large empty spaces, then the molecules are not tightly packed and a small amount of the applied external mechanical force may break the crystal easily. For checking the mechanical stability of the crystal packing, void analysis was performed by adding up the electron densities of the spherically symmetric atoms contained in the asymmetric unit [61]. The void surface is defined as an isosurface of the procrystal electron density, and calculated for the whole unit cell. Where the void surface meets the boundary of the unit cell, and the capping faces are generated to create an enclosed volume. The volumes of the crystal voids [Fig. 8a, b (for **I**), and Fig. 8c, d (for **II**)] and the percentages of free spaces in the unit cells are calculated as 58.55 $Å^3$ and 9.16% (for **I**) and 258.80 $Å^3$ and 10.30% (for **II**). Thus, there are no large cavities in the crystal packings.

## FT-IR spectroscopy results

The beneficial technique of FT-IR spectroscopy was utilized to predict the functional groups in the structures of the produced molecules [62, 63]. The υ(N–H) stretching vibrations were recorded at 3100 $cm^{-1}$ (for **I**). On the other hand, the υ(C=O) group vibrations were observed at 1666 $cm^{-1}$ (for **I**), while the stretching vibrations with υ(C=N) appeared at 1591 $cm^{-1}$ (for **I**) and 1369 $cm^{-1}$ (for **II**). For compounds (**I** and **II**), the bands associated with $υ(C–H)_{aromatic}$ vibrations were detected at 2844 $cm^{-1}$ and 2844 $cm^{-1}$, respectively. The υ(C–N) stretching vibrations of the pyridine rings were observed at 1290 $cm^{-1}$ (for **I**) and 1158 $cm^{-1}$ (for **I**). In compound **II**, the recorded chemical shifts of vibrations for the N–N and pyridine C–N groups were attributed to Cu–N bonds in 500–350 $cm^{-1}$ region, the spectra of Cu(II) complexes show two υ(Cu–N) bands, suggesting the possibility of specific vibrational couplings among Cu–N vibrations [64]. It has been found that the experimentally observed and theoretically calculated functional group vibrations are consistent with each other. (Fig. 9).

## UV–Vis spectra for schiff bases and their complexes

The electronic spectra for Schiff bases and their complexes were recorded in DMF at room temperature in the range of 200–1100 nm, as shown in Fig. S1 and S2. Electronic absorptions recorded between 250 and 370 nm were

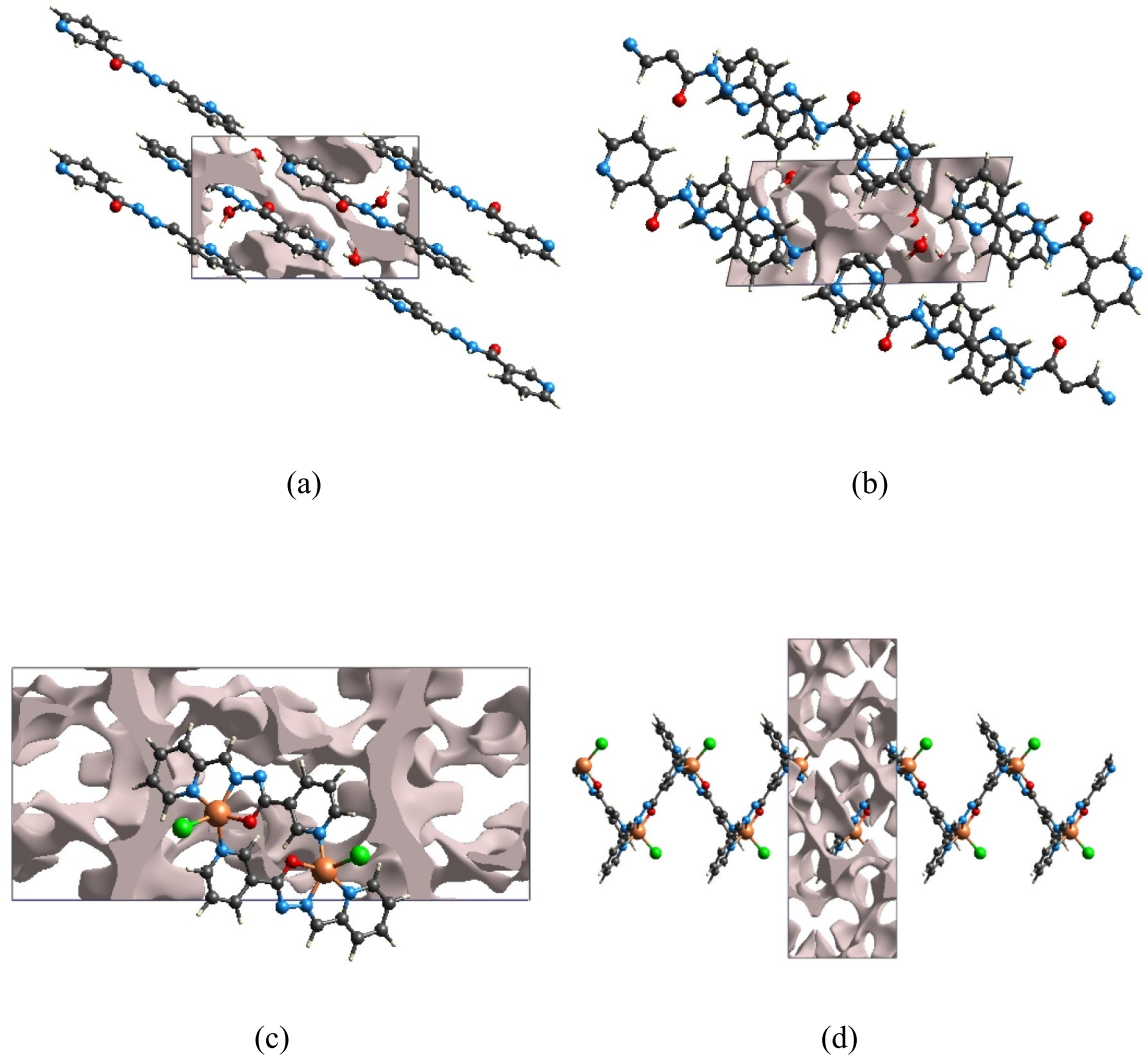



**Fig. 8** Graphical views of voids in the crystal packings of compounds viewed down (a) *a*-axis and (b) *b*-axis (for **I**) and (c) *a*-axis and (d) *b*-axis (for **II**)

attributed to the transitions of the C=N group for the imine and π–π* transitions. The peak seen in the 650–800 nm range and peaking at 701 nm is due to *d-d* electron transitions in the copper atom [3, 65].

### *$^{1}$H NMR and $^{13}$C NMR spectral studies of the compound I*

As seen in Fig. S3, the $^{1}$H, and $^{13}$C NMR spectra were characterized by sets of signals for different chemical groups present in this study. In the $^{1}$H-NMR spectra of compound **I**, the N–H proton signals were observed at 12.23 ppm. The doublet at 9.08 ppm is the aromatic C–H belonging to the pyridine ring and this is split into a doublet by long-distance interaction with another aromatic C–H (j = 1.25 Hz). The specific HC=N imine proton resonated as a singlet at 8.45 ppm. Also, aromatic protons resonated between 9.08 and 7.36 ppm. The imine proton (HC = N) resonated as a singlet at 8.45 ppm. In the $^{13}$C-NMR spectra of compound **I**, the C=O signal was seen at 162.4 ppm. Aromatic carbon signals and C=N carbon signals were observed at 120–154 ppm [62, 66–68].

## Molecular electrostatic potential (MEP) and Frontier molecular orbitals

In the context of Schiff base complexes, several studies have used DFT to elucidate their molecular properties and catalytic behavior. For example, Kargar et al. conducted a comprehensive study on a novel dioxomolybdenum Schiff base complex using DFT in conjunction with experimental methods to characterize its spectral properties

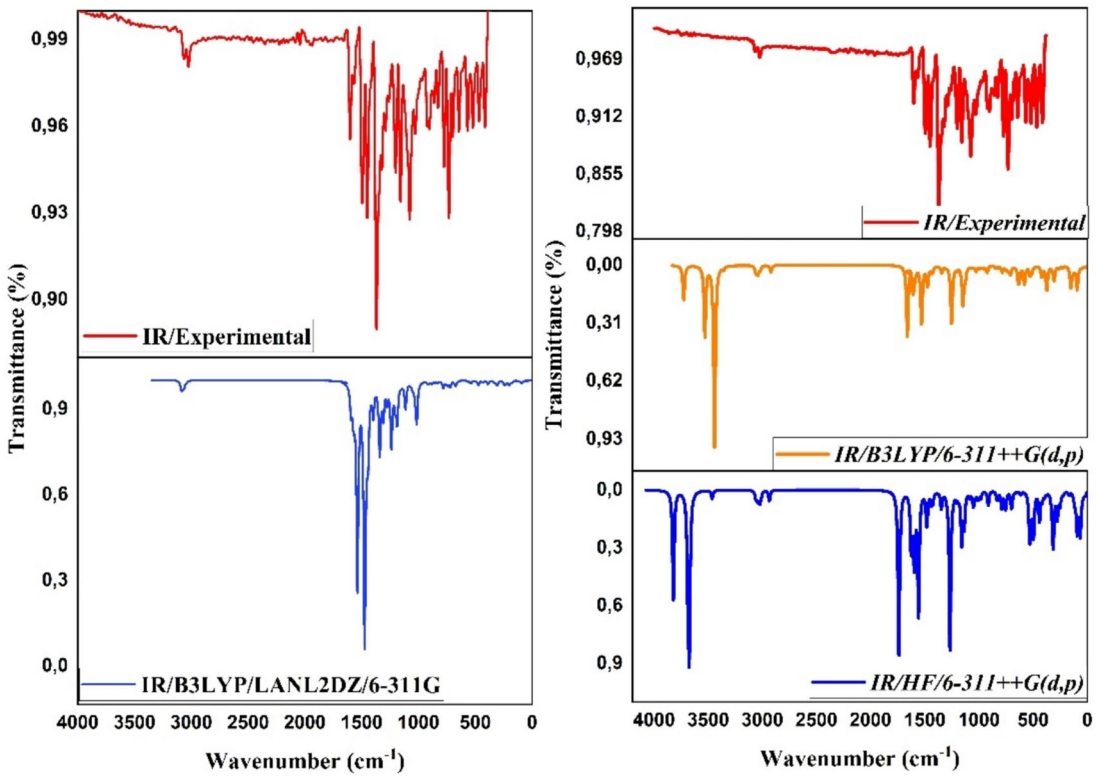



**Fig. 9** FT-IR spectra of the compounds (**I** and **II**)

**Table 4** Electronic energy, μ, α, β, $E_{HOMO,}$ and $E_{LUMO}$ of compounds (**I** and **II**)

| B3LYP/6–311 + + G(d. p) | | | | | | | |
|---|---|---|---|---|---|---|---|
| | Electronic Energy (a.u.) | μ (D) | α (a.u.) | β (a.u.) | $E_{HOMO}$ (a.u.) (a.u.) | $E_{LUMO}$(a.u.) (a.u.) | $\Delta Eg$(eV) $\Delta E_g$ = |
| I | − 910.638134964 | 4.30 | 213.98 | 977.14 | − 0.252994 | − 0.093750 | 4.333 |
| II | – | – | – | – | − 0.00284 | 0.01387 | 0.455 |
| HF/6–311 + + G(d. p) | | | | | | | |
| I | − 905.177735958 | 3.57 | 182.12 | 104.04 | − 0.331797 | 0.025863 | 9.732 |

and catalytic activity. Theoretical calculations provided insights into the electronic distribution and stability of the complex, which were confirmed by experimental findings. Similarly, the DFT approach has been applied to the study of Pd(II) complexes containing tetradentate Schiff base ligands. Kargar et al. have emphasized the importance of DFT in understanding the structural and electronic properties of these complexes, which play an important role in their activity as catalysts in reactions such as Suzuki–Miyaura cross-coupling. DFT calculations not only supported the experimental data but also provided predictions regarding the reaction mechanisms involved. Moreover, in the synthesis and characterization of dinuclear Zn(II) Schiff base complexes, DFT has been used to explore theoretical aspects of their molecular structure and antimicrobial activity. The study showed that DFT calculations are effective in predicting the stability and reactivity of these complexes, thus improving the understanding of their potential applications. In another study focusing on a dioxovanadium(V) complex, DFT was used to analyze the electronic properties and catalytic potential of the complex formed with an aminobenzohydrazone Schiff base ligand. The findings obtained from DFT calculations were reported to be very important in interpreting the experimental results and demonstrating the effectiveness of the complex in catalysis [20, 55, 69–71].

Determination of the Highest Occupied Molecular Orbital (HOMO) and the Lowest Occupied Molecular Orbital, known as frontier orbitals, is of particular importance in quantum mechanical calculations. The electronic (HOMO–LUMO) band gap is calculated using the energies of these orbitals. The electronic energy, HOMO, LUMO,

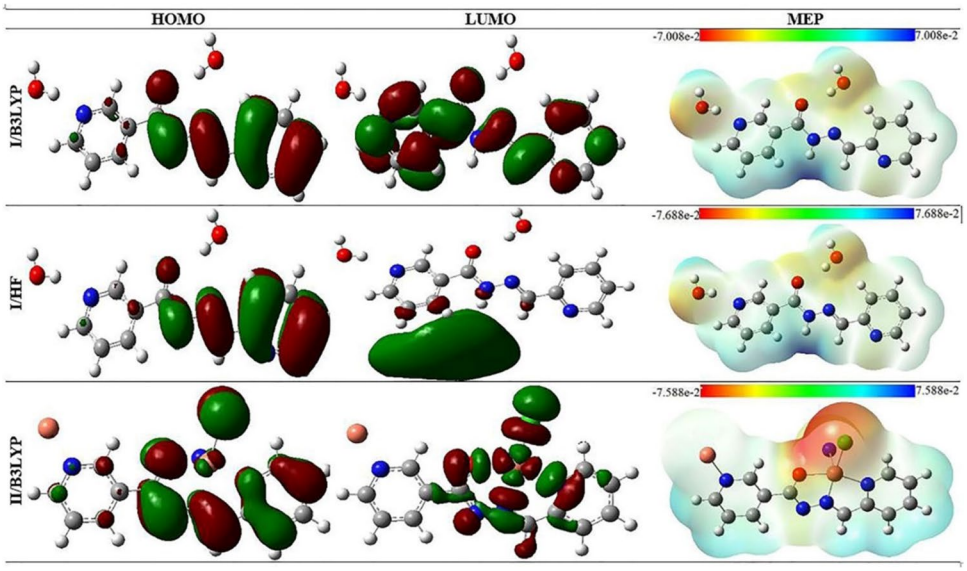



**Fig. 10** Plotted HOMO, LUMO, and MEP surfaces of compounds (**I** and **II**)

dipole moment (μ), polarizability (α) hyperpolarizability (β) values of the equilibrium state of compound **I** are calculated at B3LYP/6–311 + + G(d,p) and HF/6–311 + + G(d,p) levels of theory. For compound **II,** HOMO and LUMO values of the equilibrium state are calculated at the level of B3LYP/LANL2DZ/6-311G. The calculated molecular properties of compounds (**I** and **II**) are given in Table 4.

As seen from Table 4, the values of the electronic energy gap ($\Delta E_g = E_{LUMO} - E_{HOMO}$, where $E_{LUMO}$ and $E_{HOMO}$ are LUMO and HOMO energies) of compound **I** are 4.34 eV (B3LYP) and 9.74 eV (HF), respectively. For compound **II**, this value is 0.45 eV. The dipole moment values calculated by the same methods are 4.30 and 3.57 Debye. The $\beta$ values expressed in atomic units were converted to electrostatic units (esu) ($\beta$: 1 a.u. = $0.0086393 \times 10^{-30}$ esu) [72]. The $\beta$ values of compound **I** calculated at the B3LYP/6–311 + + G(d,p) 977.14 a.u. ($8.44 \times 10^{-30}$ esu). The hyperpolarizability value of $8.44 \times 10^{-30}$ esu is 22.69 times greater than urea. This value of the compound indicates that it may be a potential candidate in the development and application of nonlinear optical materials. The MEP, HOMO, and LUMO surfaces obtained from the calculation results are given in Fig. 10.

The HOMO orbitals of compound **I** calculated in both methods show similar behavior and the charge density is localized on N4/C8–12 ring and spacer chain between aromatic rings. LUMO orbitals calculated in both methods have not exhibited similar behavior (for B3LYP) and the charge density is localized on the entire molecule except water molecules (for HF), the charge density is located outside the molecule. The HOMO and LUMO orbitals of compound **II** show similar behavior and the charge density is localized on the entire molecule except N1/C1–C12 ring and spacer chain between aromatic rings. The color code of the compounds lies in the range of − 7.008 to $7.008e^{-2}$ (for**I**) (B3 LYP), − 7.688 to $7.688e^{-2}$ (HF), and − 7.588 to $7.588e^{-2}$ (for **II**). Red and blue colors on the MEP surface indicate more electron-rich and electron-poor regions, respectively.

## Conclusion

Schiff base ligand, *N'-(pyridine-2-ylmethylene)nicotinohydrazide* (**I**) and its Cu complex, *catena-Poly[N'-(picolinylpyridine-3-carbohydrazonate)copper(II)* (**II**) were synthesized. Their structures were characterized by single-crystal X-ray diffraction technique, FT-IR and $^{1}H$ and $^{13}C$ NMR spectroscopies, and elemental analysis. The hydrogen bonds C–H–O, N–H–O, O–H–N, and O–H–O (for **I**) and C–H–Cl interactions (for **II**) connect the molecules into a three-dimensional network. According to the Hirshfeld surface analysis results, while H–H, H–O/O–H, H–C/C–H, H–N/N–H, C–C, C–N/N–C, N–N and C–O/O–C interactions contribute to the Hirshfeld surface of both the I and II, H–Cl/Cl–H, C–Cl/Cl–C, N–O/O–N, and H–Cu/Cu–H interactions also contribute to the Hirshfeld surface of compound II. The computed band gap energy of compound **I** is 4.34 eV (at B3LYP) and 9.74 eV (at HF), respectively. For compound **II**, this value is 0.45 eV. The hyperpolarizability value of $8.44 \times 10^{-30}$ esu of compound **I** calculated at B3LYP/6–311 + + G(d,p) is 22.69 times greater than urea. This hyperpolarizability value of the compound indicates that it may be a potential candidate in the development and application of nonlinear optical materials.

**Supplementary Information** The online version contains supplementary material available at https://doi.org/10.1007/s13738-025-03177-0.

**Acknowledgements** This paper was supported by the research Fund of the Kafkas University (Project Number 2021-FM-79). TH is grateful to Hacettepe University Scientific Research Project Unit (grant No. 013 D04 602 004). The authors acknowledge to Scientific and Technological Research Application and Research Center, Sinop University, Türkiye, for the use of the Bruker D8 QUEST diffractometer.

## References

1. W. Al Zoubi, A.A.S. Al-Hamdani, M. Kaseem, Synthesis and antioxidant activities of Schiff bases and their complexes: a review. Appl. Organomet. Chem. **30**, 810–817 (2016). https://doi.org/10.1002/aoc.3506
2. M.S. Hossain, C.M. Zakaria, M. Kudrat-E-Zahan, B. Zaman, Synthesis, spectral and thermal characterization of Cu(II) complexes with two new schiff base ligand towards potential biological application. Der. Chem. Sin. **8**(3), 380–392 (2017)
3. S. Pal, A.K. Barik, S. Gupta, A. Hazra, S.K. Kar, S.-M. Peng, G.-H. Lee, R.J. Butcher, M.S. El Fallah, J. Ribas, Copper(II) mediated anion dependent formation of schiff base complexes. Inorg. Chem. Chem. **44**, 3880–3889 (2005). https://doi.org/10.1021/ic0501420
4. A.K. Patel, R.N. Jadeja, N. Patel, R.N. Patel, S.K. Patel, B. RayJ, S. Kumar, G. Kumar, Copper(II) hydrazone complexes derived from (Z)-N′-{(2-hydroxynapthalen-1-yl}methylene)acetohydrazide: synthesis, spectral characterization, electrochemical behaviour, density functional study, in vitro catalytic activity and molecular docking. Results Chem. **4**, 100244 (2022). https://doi.org/10.1016/j.rechem.2021.100244
5. F. Rhoufal, A. Laachir, S. Guesmi, L. Jouffret, N. Sergent, S. Obbade, M. Akkurt, F. Bentiss, New Cobalt(II) and Copper(II) thiocyanate complexes of 2,5-Bis(pyridin-2-yl)-1,3,4-oxadiazole ligand: synthesis, crystal structures, spectral properties and hirshfeld surface analysis. Chem. Select **4**, 7773–7783 (2019). https://doi.org/10.1002/slct.201901219
6. F. Sahan, M. Kose, C. Hepokur, D. Karakas, M. Kurtoglu, New azo-azomethine-based transition metal complexes: synthesis, spectroscopy, solid-state structure, density functional theory calculations and anticancer studies. Appl. Organomet. Chem. **33**, e4954 (2019). https://doi.org/10.1002/aoc.4954
7. T. Hokelek, F. Yilmaz, B. Tercan, F.E. Ozbek, H. Necefoglu, Bis(μ-2-fluorobenzoato-1:2κ<SUP>2</SUP>*O*:*O*′)(2-fluorobenzo ato-1κ<SUP>2</SUP>*O*,*O*′)(2-fluorobenzoato-2*κ*O)dinico tinamide-1*κ*N<SUP>1</SUP>,2*κ*N<SUP>1</SUP>-dizinc(II)-2-fluo robenzoic acid (1/1). Acta. Crystallogr. Sect. E-Crystallogr. Commun. **65**, M1608–M1983 (2009). https://doi.org/10.1107/S1600536809048089
8. T. Hökelek, H. Dal, B. Tercan, F.E. Özbek, H. Necefoğlu, Diaquabis(2-bromobenzoato-κ *O* )bis(nicotinamide-κ $N^1$)zinc(II). Acta. Crystallogr. E Struct. Rep. Online **65**, m607–m608 (2009). https://doi.org/10.1107/S1600536809015645
9. M. Pervaiz, I. Ahmad, M. Yousaf, S. Kirn, A. Munawar, Z. Saeed, A. Adnan, T. Gulzar, T. Kamal, A. Ahmad, A. Rashid, Synthesis, spectral and antimicrobial studies of amino acid derivative Schiff base metal (Co, Mn, Cu, and Cd) complexes. Spectrochim. Acta Part A Mol. Biomol. Spectrosc. **206**, 642–649 (2019). https://doi.org/10.1016/j.saa.2018.05.057
10. A. Trzesowska-Kruszynska, Copper complex of glycine Schiff base: In situ ligand synthesis, structure, spectral, and thermal properties. J. Mol. Struct. **1017**, 72–78 (2012). https://doi.org/10.1016/j.molstruc.2012.03.003
11. E. Yousif, A. Majeed, K. Al-Sammarrae, N. Salih, J. Salimon, B. Abdullah, Metal complexes of schiff base: preparation, characterization and antibacterial activity. Arab. J. Chem. **10**, S1639–S1644 (2017). https://doi.org/10.1016/j.arabjc.2013.06.006
12. T. Kondori, N. Akbarzadeh-T, M. Fazli, B. Mir, M. Dušek, V. Eigner, A novel schiff base ligand and its copper complex: synthesis, characterization, X-ray crystal structure and biological evaluation. J. Mol. Struct. **1226**, 129395 (2021). https://doi.org/10.1016/j.molstruc.2020.129395
13. E.K. Efthimiadou, H. Thomadaki, Y. Sanakis, C.P. Raptopoulou, N. Katsaros, A. Scorilas, A. Karaliota, G. Psomas, Structure and biological properties of the copper(II) complex with the quinolone antibacterial drug N-propyl-norfloxacin and 2,2'-bipyridine. J. Inorg. Biochem. **101**, 64–73 (2007). https://doi.org/10.1016/j.jinorgbio.2006.07.019
14. R. Nakagame, A. Tsaturyan, T. Haraguchi, Y. Pimonova, T. Lastovina, T. Akitsu, I. Shcherbakov, Photochemical reaction of amino acid schiff base derived Cu complexes with extended π-system and their titanium oxide composites. Inorg. Chim. Acta **486**, 221–231 (2019). https://doi.org/10.1016/j.ica.2018.10.034
15. J. Patole, U. Sandbhor, S. Padhye, D.N. Deobagkar, C.E. Anson, A. Powell, Structural chemistry and In vitro antitubercular activity of acetylpyridine benzoyl hydrazone and its copper complex against mycobacterium smegmatis. Bioorg. Med. Chem. Lett. Med. Chem. Lett. **13**, 51–55 (2003). https://doi.org/10.1016/S0960-894X(02)00855-7
16. A.A. Recio Despaigne, J.G. Da Silva, A.C.M. Do Carmo, O.E. Piro, E.E. Castellano, H. Beraldo, Copper(II) and zinc(II) complexes with 2-benzoylpyridine-methyl hydrazone. J. Mol. Struct. **920**, 97–102 (2009). https://doi.org/10.1016/j.molstruc.2008.10.025
17. P.V. Bernhardt, J. Mattsson, D.R. Richardson, Complexes of cytotoxic chelators from the dipyridyl ketone isonicotinoyl hydrazone (HPKIH) analogues. Inorg. Chem. Chem. **45**, 752–760 (2006). https://doi.org/10.1021/ic051573l
18. E. Pahlavani, H. Kargar, Synthesis, characterization, and study of anti-tubercular and anti-microbial activity of ısonicotinohydrazide tridentate schiff base ligands. Iran. J. Chem. Chem. Eng. (2021). https://doi.org/10.30492/ijcce.2019.37299
19. R. Kia, H. Kargar, Synthesis, spectral characterization and crystal structure studies of a new hydrazone Schiff base and its dioxomolybdenum(VI) complex. J. Coord. Chem. **68**, 1441–1451 (2015). https://doi.org/10.1080/00958972.2015.1011146
20. H. Kargar, M. Fallah-Mehrjardi, R. Behjatmanesh-Ardakani, K.S. Munawar, M. Ashfaq, M.N. Tahir, Synthesis, spectral characterization, SC-XRD, HSA, DFT and catalytic activity of novel dioxovanadium(V) complex with aminobenzohydrazone Schiff base ligand: an experimental and theoretical approach. Inorg. Chim. Acta **526**, 120535 (2021). https://doi.org/10.1016/j.ica.2021.120535
21. H. Kargar, M. Fallah-Mehrjardi, R. Behjatmanesh-Ardakani, K.S. Munawar, Synthesis, spectra (FT-IR, NMR) investigations, DFT, FMO, MEP, NBO analysis and catalytic activity of MoO2(VI) complex with ONO tridentate hydrazone Schiff base ligand. J. Mol. Struct. **1245**, 131259 (2021). https://doi.org/10.1016/j.molstruc.2021.131259
22. H. Kargar, M. Fallah-Mehrjardi, M. Moghadam, R. Behjatmanesh-Ardakani, A. Jamshidvand, K.S. Munawar, Synthesis, spectral characterization, and theoretical studies of oxo-peroxo tungsten (VI) Schiff base complex with an isonicotinohydrazone ligand and its application in the selective oxidation of benzylic alcohols. J. Iran. Chem. Soc. **20**, 2005–2015 (2023). https://doi.org/10.1007/s13738-023-02816-8
23. H. Kargar, M. Fallah-Mehrjardi, M. Ashfaq, K.S. Munawar, M.N. Tahir, Cis-dioxomolybdenum(VI) complex bearing tridentate

ONO isonicotinoyl hydrazone Schiff base: synthesis, characterization, crystal structure, and catalytic activity investigation for the oxidation of sulfides. J. Mol. Struct. **1294**, 136458 (2023). https://doi.org/10.1016/j.molstruc.2023.136458
24. M. Fallah-Mehrjardi, H. Kargar, K.S. Munawar, Tridentate ONO hydrazone Schiff base complexes in organic transformations: catalytic and mechanistic studies. Inorg. Chim. Acta. **560**, 121835 (2024). https://doi.org/10.1016/j.ica.2023.121835
25. H. Kargar, M. Fallah-Mehrjardi, K.S. Munawar, Metal complexes incorporating tridentate ONO pyridyl hydrazone Schiff base ligands: crystal structure, characterization and applications. Coord. Chem. Rev. **501**, 215587 (2024). https://doi.org/10.1016/j.ccr.2023.215587
26. S.K. Dey, B. Bag, K.M. Abdul Malik, M.S. El Fallah, J. Ribas, S. Mitra, A quasi-tetrahedral $Cu_4$ cluster and a helical-chain copper(II) complex with single syn−anti carboxylate bridges: crystal structure and magnetic properties. Inorg. Chem. Chem. **42**, 4029–4035 (2003). https://doi.org/10.1021/ic0206488
27. N. Zhang, Z.-L. You, Syntheses and crystal structures of two tetranuclear copper(II) complexes with Schiff bases. Transit. Met. Chem. **35**, 437–440 (2010). https://doi.org/10.1007/s11243-010-9346-1
28. J.-Y. Ma, T.-X. Wu, X.-G. She, X.-F. Pan, Crystal structure of dichloro((N-(N′, N′-dimethylammonio)ethyl)- 2,4-dichlorosalicylaldiminato-N, O)copper(II), Cu(C11H14Cl2N2O)Cl2. Zeitschrift für Kristallographie: New. Cryst. Struct. **221**, 53–54 (2006). https://doi.org/10.1524/ncrs.2006.221.1.53
29. G.M. Sheldrick, SHELXT: Integrated space-group and crystal-structure determination. Acta. Crystallogr. A. Found Adv. **71**, 3–8 (2015). https://doi.org/10.1107/S2053273314026370
30. G.M. Sheldrick, Crystal structure refinement with *SHELXL*. Acta. Crystallogr. C. Struct. Chem. **71**, 3–8 (2015). https://doi.org/10.1107/S2053229614024218
31. L.J. Farrugia, WinGX and ORTEP for Windows: an update. J. Appl. Crystallogr. **45**, 849–854 (2012). https://doi.org/10.1107/S0021889812029111
32. A.L. Spek, Structure validation in chemical crystallography. Acta Crystallogr. D Biol. Crystallogr. **65**, 148–155 (2009). https://doi.org/10.1107/S090744490804362X
33. Dennington R, Keith T, Millam J (2009) GaussView, Version 5.0.8.: Semichem Inc., Shawnee Mission KS. http://www.oalib.com/references/12626365. Accessed 15 Mar 2019
34. G09 | Gaussian.com. https://gaussian.com/glossary/g09/. Accessed 31 Jul 2021
35. P. Hohenberg, W. Kohn, Inhomogeneous electron gas. Phys. Rev. **136**, B864–B871 (1964). https://doi.org/10.1103/PhysRev.136.B864
36. W. Kohn, L.J. Sham, Self-consistent equations including exchange and correlation effects. Phys. Rev. **140**, A1133–A1138 (1965). https://doi.org/10.1103/PhysRev.140.A1133
37. A.D. Becke, Density-functional exchange-energy approximation with correct asymptotic behavior. Phys. Rev. A **38**, 3098–3100 (1988). https://doi.org/10.1103/PhysRevA.38.3098
38. A.D. Becke, Density-functional thermochemistry. III. The role of exact exchange. J. Chem. Phys. **98**, 5648–5652 (1993). https://doi.org/10.1063/1.464913
39. C. Lee, W. Yang, R.G. Parr, Development of the Colle-Salvetti correlation-energy formula into a functional of the electron density. Phys. Rev. B **37**, 785–789 (1988). https://doi.org/10.1103/PhysRevB.37.785
40. C.C.J. Roothaan, New developments in molecular orbital theory. Rev. Mod. Phys. **23**, 69–89 (1951). https://doi.org/10.1103/RevModPhys.23.69
41. R. Krishnan, J.S. Binkley, R. Seeger, J.A. Pople, Self-consistent molecular orbital methods. XX. A basis set for correlated wave functions. J. Chem. Phys. **72**, 650–654 (1980). https://doi.org/10.1063/1.438955
42. M.J. Frisch, J.A. Pople, J.S. Binkley, Self-consistent molecular orbital methods 25. Supplementary functions for Gaussian basis sets. J. Chem. Phys. **80**, 3265–3269 (1984). https://doi.org/10.1063/1.447079
43. T.R. Cundari, W.J. Stevens, Effective core potential methods for the lanthanides. J. Chem. Phys. **98**, 5555–5565 (1993). https://doi.org/10.1063/1.464902
44. W.J. Stevens, M. Krauss, H. Basch, P.G. Jasien, Relativistic compact effective potentials and efficient, shared-exponent basis sets for the third-, fourth-, and fifth-row atoms. Can. J. Chem. **70**, 612–630 (1992). https://doi.org/10.1139/v92-085
45. W.J. Stevens, H. Basch, M. Krauss, Compact effective potentials and efficient shared-exponent basis sets for the first- and second-row atoms. J. Chem. Phys. **81**, 6026–6033 (1984). https://doi.org/10.1063/1.447604
46. N. Sundaraganesan, S. Ilakiamani, H. Saleem, W. PiotrM, D. Michalska, FT-Raman and FT-IR spectra, vibrational assignments and density functional studies of 5-bromo-2-nitropyridine. Spectrochim. Acta Part A Mol. Biomol. Spectrosc. **61**, 2995–3001 (2005). https://doi.org/10.1016/j.saa.2004.11.016
47. M.H. Jamróz, Vibrational energy distribution analysis (VEDA): scopes and limitations. Spectrochim. Acta Part A Mol. Biomol. Spectrosc.. Acta Part A Mol. Biomol. Spectrosc. **114**, 220–230 (2013). https://doi.org/10.1016/j.saa.2013.05.096
48. J. Bernstein, R.E. Davis, L. Shimoni, N.-L. Chang, Patterns in hydrogen bonding: functionality and graph set analysis in crystals. Angew. Chem. Int. Ed. Engl.. Chem., Int. Ed. Engl. **34**, 1555–1573 (1995). https://doi.org/10.1002/anie.199515551
49. F.L. Hirshfeld, Bonded-atom fragments for describing molecular charge densities. Theoret. Chim. Acta **44**, 129–138 (1977). https://doi.org/10.1007/BF00549096
50. M.A. Spackman, D. Jayatilaka, Hirshfeld surface analysis. CrystEngComm **11**, 19–32 (2009). https://doi.org/10.1039/B818330A
51. M. J. Turner, J. J. McKinnon, S. K. Wolff, D. J. Grimwood, P. R. Spackman, D. Jayatilaka and M. A. Spackman, CrystalExplorer17 (2017). University of Western Australia.
52. P. Venkatesan, S. Thamotharan, A. Ilangovan, H. Liang, T. Sundius, Crystal structure, Hirshfeld surfaces and DFT computation of NLO active (2E)-2-(ethoxycarbonyl)-3-[(1-methoxy-1-oxo-3-phenylpropan-2-yl)amino] prop-2-enoic acid. Spectrochim. Acta Part A Mol. Biomol. Spectrosc. **153**, 625–636 (2016). https://doi.org/10.1016/j.saa.2015.09.002
53. J.J. McKinnon, D. Jayatilaka, M.A. Spackman, Towards quantitative analysis of intermolecular interactions with Hirshfeld surfaces. Chem. Commun. (2007). https://doi.org/10.1039/b704980c
54. V.R. Hathwar, M. Sist, M.R.V. Jørgensen, A.H. Mamakhel, X. Wang, C.M. Hoffmann, K. Sugimoto, J. Overgaard, B.B. Iversen, Quantitative analysis of intermolecular interactions in orthorhombic rubrene. IUCrJ **2**, 563–574 (2015). https://doi.org/10.1107/S2052252515012130
55. H. Kargar, M. Fallah-Mehrjardi, R. Behjatmanesh-Ardakani, M. Bahadori, M. Moghadam, M. Ashfaq, K.S. Munawar, M.N. Tahir, Spectroscopic investigation, molecular structure, catalytic activity with computational studies of a novel Pd(II) complex incorporating unsymmetrical tetradentate Schiff base ligand. Inorg. Chem. Commun. **142**, 109697 (2022). https://doi.org/10.1016/j.inoche.2022.109697
56. H. Kargar, M. Ashfaq, M. Fallah-Mehrjardi, R. Behjatmanesh-Ardakani, K.S. Munawar, M.N. Tahir, Synthesis, characterization, SC-XRD, HSA and DFT study of a novel copper(I) iodide complex with 2-(thiophen-2-yl)-4,5-dihydro-1H-imidazole ligand: an experimental and theoretical approach. J. Mol. Struct. **1253**, 132264 (2022). https://doi.org/10.1016/j.molstruc.2021.132264

57. M. Fallah-Mehrjardi, H. Kargar, R. Behjatmanesh-Ardakani, M. Ashfaq, K.S. Munawar, M.N. Tahir, Symmetrical Pd(II) and Ni(II) Schiff base complexes: synthesis, crystal structure determination, spectral characterization, and theoretical studies. J. Mol. Struct. **1251**, 132037 (2022). https://doi.org/10.1016/j.molstruc.2021.132037
58. H. Kargar, M. Fallah-Mehrjardi, R. Behjatmanesh-Ardakani, K.S. Munawar, M. Ashfaq, M.N. Tahir, Experimental and theoretical studies of new dioxomolybdenum complex: synthesis, characterization and application as an efficient homogeneous catalyst for the selective sulfoxidation. Inorg. Chim. Acta **527**, 120568 (2021). https://doi.org/10.1016/j.ica.2021.120568
59. H. Kargar, M. Fallah-Mehrjardi, R. Behjatmanesh-Ardakani, K.S. Munawar, M. Ashfaq, M.N. Tahir, Diverse coordination of isoniazid hydrazone Schiff base ligand towards iron(III): synthesis, characterization, SC-XRD, HSA, QTAIM, MEP, NCI, NBO and DFT study. J. Mol. Struct. **1250**, 131691 (2022). https://doi.org/10.1016/j.molstruc.2021.131691
60. H. Kargar, M. Fallah-Mehrjardi, R. Behjatmanesh-Ardakani, K.S. Munawar, M. Ashfaq, M.N. Tahir, Titanium(IV) complex containing ONO-tridentate Schiff base ligand: synthesis, crystal structure determination, Hirshfeld surface analysis, spectral characterization, theoretical and computational studies. J. Mol. Struct. **1241**, 130653 (2021). https://doi.org/10.1016/j.molstruc.2021.130653
61. M.J. Turner, J.J. McKinnon, D. Jayatilaka, M.A. Spackman, Visualisation and characterisation of voids in crystalline materials. CrystEngComm **13**, 1804–1813 (2011). https://doi.org/10.1039/C0CE00683A
62 D.L. Pavia, G.M. Lampman, G.S. Kriz, *Introduction to spectroscopy: a guide for students of organic chemistry*, 3rd edn. (Brooks/Cole, South Melbourne, 2001)
63. B.H. Stuart, *Infrared spectroscopy: fundamentals and applications* (Wiley, Chichester, 2008)
64. M. Kumru, T. Bardakçı, S. Güner, DFT calculations and experimental FT-IR, dispersive-Raman and EPR spectral studies of Copper (II) chloride complex with 3-amino-1-methylbenzene. Spectrochim. Acta Part A Mol. Biomol. Spectrosc. **123**, 187–193 (2014). https://doi.org/10.1016/j.saa.2013.12.068
65. H. Suzuki, *Electronic absorption spectra and geometry of organic molecules an application of molecular orbital theory* (Elsevier Science, Burlington, 2012)
66. M.M. Alqasaimeh, A.-A.M. Abu-Yamin, S.A. Matar, I.A. Saraairah, M.M. Salman, Synthesis and characterization of a new Schiff-base derivative as an optical nickel (II) chemosensor and its antimicrobial activity. J. Photochem. Photobiol., A **447**, 115277 (2024). https://doi.org/10.1016/j.jphotochem.2023.115277
67. F.E. Öztürkkan Özbek, G. Uğurlu, E. Kalay, H. Necefoğlu, T. Hökelek, Theoretical and experimental assesment of structural, spectroscopic, electronic and nonlinear optical properties of two aroylhydrazone derivative. J. Mol. Struct. **1223**, 128982 (2021). https://doi.org/10.1016/j.molstruc.2020.128982
68. F. Elif Öztürkkan Özbek, G. Uğurlu, E. Kalay, H. Necefoğlu, Synthesis, characterization and computational studies of 4-[(Pyridine-3-carbonyl)-hydrazonomethyl]-benzoic acid. J. Mol. Struct. **1215**, 128247 (2020). https://doi.org/10.1016/j.molstruc.2020.128247
69. H. Kargar, M. Nateghi-Jahromi, M. Fallah-Mehrjardi, R. Behjatmanesh-Ardakani, K.S. Munawar, S. Ali, M. Ashfaq, M.N. Tahir, Synthesis, spectral characterization, crystal structure and catalytic activity of a novel dioxomolybdenum Schiff base complex containing 4-aminobenzhydrazone ligand: a combined experimental and theoretical study. J. Mol. Struct. **1249**, 131645 (2022). https://doi.org/10.1016/j.molstruc.2021.131645
70. H. Kargar, M. Fallah-Mehrjardi, R. Behjatmanesh-Ardakani, H.A. Rudbari, A.A. Ardakani, S. Sedighi-Khavidak, K.S. Munawar, M. Ashfaq, M.N. Tahir, Binuclear Zn(II) Schiff base complexes: synthesis, spectral characterization, theoretical studies and antimicrobial investigations. Inorg. Chim. Acta **530**, 120677 (2022). https://doi.org/10.1016/j.ica.2021.120677
71. H. Kargar, M. Fallah-Mehrjardi, R. Behjatmanesh-Ardakani, H. Amiri Rudbari, A. Adabi Ardakani, S. Sedighi-Khavidak, K.S. Munawar, M. Ashfaq, M.N. Tahir, Synthesis, spectral characterization, crystal structures, biological activities, theoretical calculations and substitution effect of salicylidene ligand on the nature of mono and dinuclear Zn(II) Schiff base complexes. Polyhedron **213**, 115636 (2022). https://doi.org/10.1016/j.poly.2021.115636
72. I.C. De Silva, R.M. De Silva, K.M. Nalin De Silva, Investigations of nonlinear optical (NLO) properties of Fe, Ru and Os organometallic complexes using high accuracy density functional theory (DFT) calculations. J. Mol. Struct. (Thoechem) **728**, 141–145 (2005). https://doi.org/10.1016/j.theochem.2005.02.092


Springer Nature or its licensor (e.g. a society or other partner) holds exclusive rights to this article under a publishing agreement with the author(s) or other rightsholder(s); author self-archiving of the accepted manuscript version of this article is solely governed by the terms of such publishing agreement and applicable law.

## Authors and Affiliations


**Ömer Aydoğdu[1] · Füreya Elif Öztürkkan[2] · Tuncer Hökelek[3] · Güventürk Uğurlu[4] · Hacali Necefoğlu[1,5]**

✉ Füreya Elif Öztürkkan
fozturkkan36@gmail.com

[1] Department of Chemistry, Kafkas University, 36100 Kars, Türkiye

[2] Department of Chemical Engineering, Kafkas University, 36100 Kars, Türkiye

[3] Department of Physics, Hacettepe University, 06800 Ankara, Türkiye

[4] Department of Physics, Kafkas University, 36100 Kars, Türkiye

[5] Department of Inorganic Chemistry and Materials Science, Institute of Biochemistry, Samarkand State University, 140104 Samarkand, Uzbekistan